COUPLED BEM-FEM METHODS FOR 3D FIELD CALCULATIONS WITH IRON SATURATION

S. Kurz, J. Fetzer, W.M. Rucker
Universität Stuttgart, Institut für Theorie der Elektrotechnik,
Germany

Abstract
If electromagnetic problems are solved by finite elements, the computation for problems involving infinite space and/or complicated coil geometries causes difficulties. One possibility to treat such problems is the coupling of finite elements (FEM) and boundary elements (BEM), referred to as BEM-FEM coupling. The physical problem is decomposed into a BEM part, which represents the surrounding space as well as prescribed exciting currents, and a FEM part, which contains the magnetic media. In this paper, the BEM-FEM coupling for magnetostatic problems is derived in detail. For the treatment of nonlinear media the $M(B)$-iteration is presented. As an application example the computation of iron induced effects in superconducting dipole magnets is considered.

1 Introduction

Magnetostatic problems are described by Maxwell's equations

$$\operatorname{curl} \vec{H} = \vec{j}_{\mathrm{s}}, \tag{1}$$

$$\operatorname{div} \vec{B} = 0 \tag{2}$$

and by the constitutive relation

$$\vec{B} = \mu_0 \vec{H} + \mu_0 \vec{M}, \tag{3}$$

where $\vec{H}$ is the magnetic field, $\vec{j}_{\mathrm{s}}$ the impressed source current density, $\vec{B}$ the flux density and $\vec{M}$ the magnetization. The magnetization is assumed to be of the form

$$\vec{M} = \left(\frac{B(H)}{\mu_0 H} - 1 \right) \vec{H}, \tag{4}$$

where $B(H)$ is some single-valued monotonous nonlinear magnetization curve. A permanent magnetization $\vec{M}_0$ could be easily added to (4). From (1) we have

$$\operatorname{div} \vec{j}_{\mathrm{s}} = 0 \tag{5}$$

for all currents.
By introducing the potential $\vec{A}$ the usual way,

$$\vec{B} = \operatorname{curl} \vec{A}, \tag{6}$$

(1) – (3) can be equivalently expressed as

$$\vec{\Delta} \vec{A} = -\mu_0 \left(\vec{j}_{\mathrm{s}} + \operatorname{curl} \vec{M} \right). \tag{7}$$

It can be shown [1] that (5) and (7) in connection with the condition $\vec{A} = 0$ at infinity imply the Coulomb gauge

$$\operatorname{div} \vec{A} = 0. \tag{8}$$

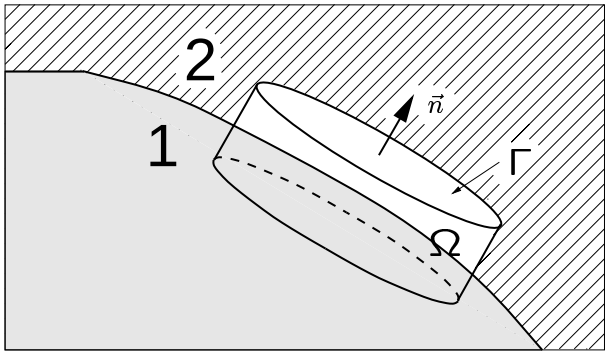

Fig. 1: Integration over a small cylindrical volume Ω with the boundary Γ

From the equations given so far some interface conditions for the vector potential and its derivatives can be derived. This will be explained in greater detail, because these interface conditions are of fundamental importance for the application of the BEM-FEM coupling. For the differential operators curl and div in (6) and (8) to make sense, the vector potential has to be continuous,

$$\left[\vec{A}\right] = 0. \tag{9}$$

The brackets denote the jump of their argument across a surface of discontinuity in the direction of $\vec{n}$, the unit normal vector. An immediate consequence of (9) is

$$\vec{n} \cdot \left[\vec{B}\right] = 0. \tag{10}$$

If we integrate (7) over a small cylindrical volume according to Figure 1 and take into account $-\vec{\Delta}\vec{A} = \mathrm{curl}\,\mathrm{curl}\,\vec{A} - \mathrm{grad}\,\mathrm{div}\,\vec{A}$ and the identities [2]

$$\int_{\Omega} \mathrm{curl}\,\vec{a}\,\mathrm{d}\Omega = \oint_{\Gamma=\partial\Omega} \vec{n} \times \vec{a}\,\mathrm{d}\Gamma, \tag{11}$$

$$\int_{\Omega} \mathrm{grad}\,f\,\mathrm{d}\Omega = \oint_{\Gamma=\partial\Omega} \vec{n} f\,\mathrm{d}\Gamma \tag{12}$$

we obtain the following equation,

$$\oint_{\Gamma} \left(\vec{n} \times \mathrm{curl}\,\vec{A} - \vec{n}\,\mathrm{div}\,\vec{A}\right)\,\mathrm{d}\Gamma = \int_{\Omega} \mu_0 \vec{j}_{\mathrm{s}}\,\mathrm{d}\Omega + \oint_{\Gamma} \mu_0 \vec{n} \times \vec{M}\,\mathrm{d}\Gamma. \tag{13}$$

If the height of the cylinder tends to zero, only the surfaces parallel to the interface contribute to the surface integrals in (13). Because (13) is valid for cylinders of arbitrary shape, we find for the integrands

$$\vec{n} \times \left[\mathrm{curl}\,\vec{A}\right] = \mu_0 \vec{k} + \mu_0 \vec{n} \times \left[\vec{M}\right], \tag{14}$$

$$\left[\mathrm{div}\,\vec{A}\right] = 0, \tag{15}$$

where $\vec{k}$ is a possible surface current density. Equation (14) is the usual interface condition for $\vec{H}$, namely

$$\vec{n} \times [\vec{H}\,] = \vec{k}, \tag{16}$$

equation (15) the continuity of $\mathrm{div}\,\vec{A}$. Using the identity [2]

$$\oint_{\Gamma} \left(\vec{n} \times \mathrm{curl}\,\vec{A} - \vec{n}\,\mathrm{div}\,\vec{A}\right)\,\mathrm{d}\Gamma = -\oint_{\Gamma} \frac{\partial \vec{A}}{\partial n}\,\mathrm{d}\Gamma \tag{17}$$

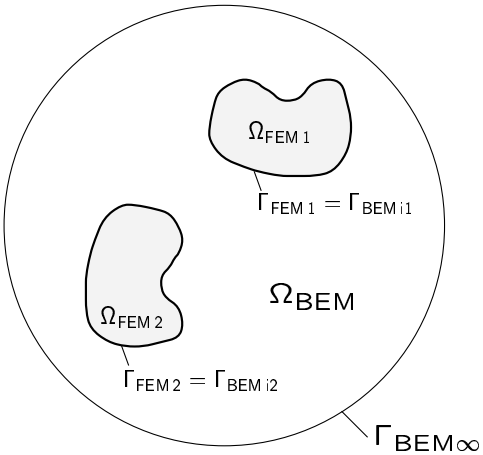

Fig. 2: Decomposition of the domain Ω into subdomains Ω_{BEM} and $\Omega_{\mathrm{FEM}\nu}$, $\nu = 1, 2$

both interface conditions can be combined to

$$\left[\frac{\partial \vec{A}}{\partial n}\right] + \mu_0 \vec{n} \times \left[\vec{M}\right] = -\mu_0 \vec{k}. \tag{18}$$

With the definition

$$\vec{Q} = \frac{\partial \vec{A}}{\partial n} + \vec{n} \times \mu_0 \vec{M}, \quad \vec{n} = \vec{n}_{\mathrm{FEM}} \tag{19}$$

we can write

$$\left[\vec{Q}\right] = 0, \tag{20}$$

where $\vec{k} = 0$ has been assumed. Surface currents will not be taken into account any longer.
If we take the dot product of $\vec{e}_z$ with (7), (9), (19) and (20), we find for the z-components

$$\Delta A_z = -\mu_0 \left(j_{z\mathrm{s}} + \vec{e}_z \cdot \operatorname{curl} \vec{M}\right), \tag{21}$$

$$\left[A_z\right] = 0, \tag{22}$$

$$Q_z = \frac{\partial A_z}{\partial n} + \left(\mu_0 \vec{M} \times \vec{e}_z\right) \cdot \vec{n}, \tag{23}$$

$$\left[Q_z\right] = 0. \tag{24}$$

The equations for the other Cartesian components can be obtained by replacing the index z by x and y, respectively. The equations (21) – (24) for the Cartesian components of $\vec{A}$ and $\vec{Q}$ are completely decoupled and can be treated separately. A mutual coupling comes into play by the magnetization $\vec{M}$, which appears on the right hand side of (21) and (23).

2 The BEM-FEM Coupling

Figure 2 shows the typical decomposition of the domain Ω which is applied for BEM-FEM coupling. The infinite domain Ω is decomposed into a subdomain Ω_{BEM} and (several) subdomains $\Omega_{\mathrm{FEM}\nu}$ with the common boundaries $\Gamma_{\mathrm{FEM}\nu} = \Gamma_{\mathrm{BEMi}\nu}$.
Subdomains which consist of magnetic media are discretized with the help of the finite element method. Those parts which contain impressed exciting currents $\vec{j}_{\mathrm{s}}$ can be described either by the finite element

method or by the boundary element method. However, in the case of complicated exciting coils it is better to avoid their modelling in the FE-mesh. The remaining domain is treated by the boundary element method in any case. In the example of Figure 2 we have

$$\Omega = \Omega_{\mathrm{FEM}} \cup \Omega_{\mathrm{BEM}}, \tag{25}$$

$$\Omega_{\mathrm{FEM}} = \Omega_{\mathrm{FEM1}} \cup \Omega_{\mathrm{FEM2}}, \tag{26}$$

$$\Gamma_{\mathrm{FEM}} = \Gamma_{\mathrm{FEM1}} \cup \Gamma_{\mathrm{FEM2}}, \quad \Gamma_{\mathrm{BEMi}} = \Gamma_{\mathrm{BEMi1}} \cup \Gamma_{\mathrm{BEMi2}}. \tag{27}$$

On the common boundary $\Gamma_{\mathrm{FEM}} = \Gamma_{\mathrm{BEMi}}$, the coupling interface, the interface conditions (9) and (20) are valid.

3 The Finite Element Description

The starting point for the finite element description is the weak integral form of (21) in the domain Ω_{FEM}. The weak integral form is obtained by multiplying (21) by a weighting function w and integrating by parts. This results in

$$\begin{aligned} &\int_{\Omega_{\mathrm{FEM}}} \operatorname{grad} A_z \cdot \operatorname{grad} w \,\mathrm{d}\Omega - \oint_{\Gamma_{\mathrm{FEM}}} Q_z \, w \,\mathrm{d}\Gamma \\ &= \int_{\Omega_{\mathrm{FEM}}} \mu_0 j_{z\mathrm{s}} \, w \,\mathrm{d}\Omega - \int_{\Omega_{\mathrm{FEM}}} \left(\mu_0 \vec{M} \times \vec{e}_z\right) \cdot \operatorname{grad} w \,\mathrm{d}\Omega, \end{aligned} \tag{28}$$

where Q_z is defined in (23). The weak integral form (28) automatically fulfills the interface condition (24) at possible interfaces in the interior of Ω_{FEM}, e.g. at the interfaces between the finite elements. The boundary integral in (28) allows to prescribe Q_z on Γ_{FEM} and therefore the coupling with the boundary element method.

At this point the discretization of the domain Ω_{FEM} into individual finite elements Ω_e takes place. Possible material interfaces must coincide with element interfaces. We use C^0-continuous, isoparametric nodal finite elements. The functions $A_z(\vec{x})$ and $Q_z(\vec{x})$ are expanded with respect to the element shape functions $N_j(\vec{x})$ and the nodal values A_{zj} and Q_{zj} as follows

$$A_z(\vec{x}) = \sum_{j=1}^{n} N_j(\vec{x}) A_{zj} \quad \text{in } \Omega_e, \tag{29}$$

$$Q_z(\vec{x}) = \sum_{j=1}^{m} N_j(\vec{x}) Q_{zj} \quad \text{on } \Gamma_{\mathrm{FEM}} \cap \Gamma_e, \tag{30}$$

where n is the number of nodes of the element Ω_e and m is the number of nodes on $\Gamma_{\mathrm{FEM}} \cap \Gamma_e$. This is the portion of the element boundary Γ_e in common with the boundary Γ_{FEM}.

If we introduce (29) and (30) into (28) and choose the weighting functions w equal to the element shape functions N_i we obtain the Galerkin equation for one finite element. Using matrix notation this equation reads

$$\big[k\big]\big\{A_z\big\} - \big[t\big]\big\{Q_z\big\} = \big\{f_z(\vec{M})\big\}, \tag{31}$$

$\big[k\big]$ = $n \times n$ element stiffness matrix,
$\big\{A_z\big\}$ = n nodal unknowns A_z in $\bar{\Omega}_e$,
$\big[t\big]$ = $n \times m$ element boundary matrix,
$\big\{Q_z\big\}$ = m nodal unknowns Q_z on $\Gamma_{\mathrm{FEM}} \cap \Gamma_e$,
$\big\{f_z(\vec{M})\big\}$ = element force n-vector.

The $m \times m$ matrix $\big[t\big]$ has been supplemented to become a $n \times m$ matrix. The global system of equations, accumulated of the element matrices and vectors according to (31) is

$$\big[K^{\mathrm{FEM}}\big]\big\{A_z\big\} - \big[T\big]\big\{Q_z\big\} = \big\{F_z^{\mathrm{FEM}}(\vec{M})\big\}, \tag{32}$$

$\big[K^{\mathrm{FEM}}\big]$ = $N \times N$ global stiffness matrix,
$\big\{A_z\big\}$ = N nodal unknowns A_z in $\bar{\Omega}_{\mathrm{FEM}}$,
$\big[T\big]$ = $N \times M$ global boundary matrix,
$\big\{Q_z\big\}$ = M nodal unknowns Q_z on Γ_{FEM},
$\big\{F_z(\vec{M})\big\}$ = global force N-vector.

In (32), N is the number of nodes in $\bar{\Omega}_{\mathrm{FEM}}$ and M is the number of nodes on Γ_{FEM}. The bar notation indicates the closure of a domain, i.e. the domain and its boundary.

4 The Boundary Element Description

Per definition the domain Ω_{BEM} contains no magnetic media, hence $\vec{M} = 0$. One more integration of (28) by parts yields

$$\int\limits_{\Omega_{\mathrm{BEM}}} A_z \Delta w \,\mathrm{d}\Omega + \oint\limits_{\Gamma_{\mathrm{BEMi}}} \left(\frac{\partial A_z}{\partial n} w - A_z \frac{\partial w}{\partial n} \right) \mathrm{d}\Gamma = \int\limits_{\Omega_{\mathrm{BEM}}} -\mu_0 j_{zs}\, w \,\mathrm{d}\Omega. \tag{33}$$

In (33) it was already taken into account that the boundary integrals over the far boundary Γ_∞ do not contribute [3]. Now the weighting function w is chosen as the fundamental solution u^* of the Laplace equation, which is in 2D

$$u^*(\vec{x}, \vec{\xi}) = -\frac{1}{2\pi} \ln |\vec{x} - \vec{\xi}| \tag{34}$$

and in 3D

$$u^*(\vec{x}, \vec{\xi}) = \frac{1}{4\pi |\vec{x} - \vec{\xi}|}. \tag{35}$$

In (34) and (35), $\vec{x}$ is the source point and $\vec{\xi}$ is the field point. With the abbreviation

$$q^*(\vec{x}, \vec{\xi}) = \frac{\partial u^*}{\partial n_{\vec{x}}} \tag{36}$$

we obtain from (33)

$$c(\vec{\xi}) A_z(\vec{\xi}) + \oint\limits_{\Gamma_{\mathrm{BEMi}}} \left(-\frac{\partial A_z}{\partial n} u^* + A_z\, q^* \right) \mathrm{d}\Gamma = \int\limits_{\Omega_{\mathrm{BEM}}} \mu_0 j_{zs}\, u^* \,\mathrm{d}\Omega. \tag{37}$$

In (37)

$$c(\vec{\xi}) = \frac{\alpha}{2\pi} \text{ in 2D and } c(\vec{\xi}) = \frac{\Theta}{4\pi} \text{ in 3D} \tag{38}$$

is the so called edge factor and α the planar angle (Θ the solid angle) at the point $\vec{\xi}$ in the interior of the domain Ω_{BEM}. The integral on the right hand side of (37) can be identified as the z-component of the Biot-Savart integral for the vector potential due to the imposed current density $\vec{j}_{\mathrm{s}}$ in Ω_{BEM},

$$\vec{A}_{\mathrm{s}}(\vec{\xi}) = \int\limits_{\Omega_{\mathrm{BEM}}} \mu_0 \vec{j}_{\mathrm{s}}\, u^* \,\mathrm{d}\Omega. \tag{39}$$

The normal derivative of the vector potential can be expressed in terms of Q_z according to (23) with $\vec{M} = 0$ in Ω_{BEM}. Furthermore, the normal derivative in (23) refers to the outward normal $\vec{n} = \vec{n}_{\mathrm{FEM}}$, wheras the outward normal $\vec{n} = \vec{n}_{\mathrm{BEM}}$ in (37) points into the opposite direction, which leads to an additional minus sign. From (23), (37), (39) and this consideration we obtain

$$c(\vec{\xi})A_z(\vec{\xi}) + \oint\limits_{\Gamma_{\mathrm{BEMi}}} Q_z\, u^*\,\mathrm{d}\Gamma + \oint\limits_{\Gamma_{\mathrm{BEMi}}} A_z\, q^*\,\mathrm{d}\Gamma = A_{z\mathrm{s}}(\vec{\xi}), \quad \vec{\xi} \in \Gamma_{\mathrm{BEMi}}. \tag{40}$$

Due to the special choice of $\vec{\xi}$ on Γ_{BEMi} only boundary values of A_z and Q_z are related to each other. Equation (40) is the integral equation on which the boundary element method is based on.
For the numerical solution of (40), the boundary Γ_{BEMi} must be decomposed into a number of E boundary elements Γ_e resulting in

$$c(\vec{\xi})A_z(\vec{\xi}) + \sum_{e=1}^{E} \int\limits_{\Gamma_e} Q_z\, u^*\,\mathrm{d}\Gamma + \sum_{e=1}^{E} \int\limits_{\Gamma_e} A_z\, q^*\,\mathrm{d}\Gamma = A_{z\mathrm{s}}(\vec{\xi}). \tag{41}$$

Again, C^0-continuous, isoparametric nodal elements are used for the discretization. These elements have exactly the same properties as the finite elements in section 3. Due to the boundary integral formulation, the dimension of the elements is reduced by one so that for 3D problems 2D boundary elements and for 2D problems 1D boundary elements have to be applied. The trial functions for A_z and Q_z for one element Γ_e are similar to those in (29) and (30),

$$A_z(\vec{x}) = \sum_{j=1}^{m} N_j(\vec{x}) A_{zj} \quad \text{on } \Gamma_e, \tag{42}$$

$$Q_z(\vec{x}) = \sum_{j=1}^{m} N_j(\vec{x}) Q_{zj} \quad \text{on } \Gamma_e, \tag{43}$$

where m is the number of nodes of the element Γ_e. If we introduce (42) and (43) into (41) and put the field point $\vec{\xi}$ succesively at the location of each boundary node $\vec{x}_k$, $k = 1 \ldots M$, we end up with a system of M equations which reads

$$\big[H\big]\big\{A_z\big\} + \big[G\big]\big\{Q_z\big\} = \big\{A_{z\mathrm{s}}\big\}, \tag{44}$$

$\big[H\big]$ = $M \times M$ matrix resulting from $q^*(\vec{x}, \vec{\xi})$,
$\big\{A_z\big\}$ = M nodal unknowns A_z on Γ_{BEMi},
$\big[G\big]$ = $M \times M$ matrix resulting from $u^*(\vec{x}, \vec{\xi})$,
$\big\{Q_z\big\}$ = M nodal unknowns Q_z on Γ_{BEMi},
$\big\{A_{z\mathrm{s}}\big\}$ = M-vector of the source potential.

This is the pointwise collocation method, which leads to unsymmetric matrices $\big[G\big]$ and $\big[H\big]$. In contrast to the symmetric sparse FEM matrices $\big[K\big]$ and $\big[T\big]$, the BEM matrices are unsymmetric and fully populated.

5 The Overall System of Equations

The boundary conditions (22) and (24) require A_z and Q_z to be continuous on the coupling interface $\Gamma_{\mathrm{FEM}} = \Gamma_{\mathrm{BEMi}}$. If "compatible" elements [4] are used in both subdomains, this is guaranteed by the continuity of the nodal values and the similar expansions (29), (42) and (30), (43), respectively.
Multiplying (44) by $\big[G\big]^{-1}$ results in

$$\big\{Q_z\big\} = -\big[G\big]^{-1}\big[H\big]\big\{A_z\big\} + \big[G\big]^{-1}\big\{A_{z\mathrm{s}}\big\}. \tag{45}$$

This equation can be used to eliminate the unknowns $\{Q_z\}$ from (32), which now reads

$$[K]\{A_z\} = \{F_z(\vec{A}_\mathrm{s}, \vec{M})\}, \tag{46}$$

$$[K] = [K^{\mathrm{FEM}}] + [K^{\mathrm{BEM}}], \tag{47}$$

$$[K^{\mathrm{BEM}}] = [T]\,[G]^{-1}[H], \tag{48}$$

$$\{F_z(\vec{A}_\mathrm{s}, \vec{M})\} = \{F_z^{\mathrm{FEM}}(\vec{M})\} + [T]\,[G]^{-1}\{A_{z\mathrm{s}}\}. \tag{49}$$

The $N \times M$ matrix $[K^{\mathrm{BEM}}]$ has been supplemented to become a $N \times N$ matrix. The domain Ω_{BEM} has been mapped onto one equivalent finite element resulting in $[K^{\mathrm{BEM}}]$. The matrix $[K^{\mathrm{BEM}}]$ is unsymmetric which means that $[K]$ is unsymmetric, too. In contrast to the sparse matrix $[K^{\mathrm{FEM}}]$, the matrix $[K]$ contains a dense $M \times M$ subblock which couples all the boundary nodes with each other. These properties of $[K]$ reduce the efficiency of the numerical solution of (46) and have to be regarded as disadvantages of the BEM-FEM coupling [4]. However, there are some special solution algorithms not explained in this paper which allow to work around these difficulties [5, 6].
The equations (46) for the Cartesian components of the vector potential may now be combined into

$$\underbrace{\begin{pmatrix} [K] & 0 & 0 \\ 0 & [K] & 0 \\ 0 & 0 & [K] \end{pmatrix}}_{[\tilde{K}]} \underbrace{\begin{pmatrix} \{A_x\} \\ \{A_y\} \\ \{A_z\} \end{pmatrix}}_{\{\vec{A}\}} = \underbrace{\begin{pmatrix} \{F_x(\vec{A}_\mathrm{s}, \vec{M})\} \\ \{F_y(\vec{A}_\mathrm{s}, \vec{M})\} \\ \{F_z(\vec{A}_\mathrm{s}, \vec{M})\} \end{pmatrix}}_{\{\vec{F}(\vec{A}_\mathrm{s}, \vec{M})\}}. \tag{50}$$

Equation (50) describes any magnetostatic problem on an infinite domain with the boundary condition $\vec{A} = 0$ at infinity.

6 The $\mathrm{M}(\mathrm{B})$-Iteration

The magnetization $\vec{M}$ which appears on the right hand side of (50) is in general not known in advance, but depends itself on the fields according to the magnetization curve (4). This means that (50) has to be solved by iteration.
A possible iterative method is the $M(B)$-iteration. The principle of the $M(B)$-iteration is a simple update. The magnetization $\vec{M}_k$ is obtained from the vector potential $\{\vec{A}_k\}$ of the current iteration step k with the help of the magnetization curve (4). The vector potential is recomputed from this magnetization in the next iteration step,

$$[\tilde{K}]\{\vec{A}_{k+1}\} = \{\vec{F}(\vec{A}_\mathrm{s}, \vec{M}_k)\}, \quad k = 0, 1, 2, \ldots\ . \tag{51}$$

If we subtract $[\tilde{K}]\{\vec{A}_k\}$ from both sides of (51) we obtain

$$[\tilde{K}]\{\delta\vec{A}_k\} = \{\vec{R}_k\}, \tag{52}$$

$$\{\vec{R}_k\} = \{\vec{F}(\vec{A}_\mathrm{s}, \vec{M}_k)\} - [\tilde{K}]\{\vec{A}_k\}, \tag{53}$$

$$\{\vec{A}_{k+1}\} = \{\vec{A}_k\} + \{\delta\vec{A}_k\}, \tag{54}$$

where $\{\delta\vec{A}_k\}$ is the increment of the potential values and $\{\vec{R}_k\}$ is the residual. The convergence rate can be improved by multiplying the increment $\{\delta\vec{A}_k\}$ by a relaxation parameter ω_k. Equation (54) has

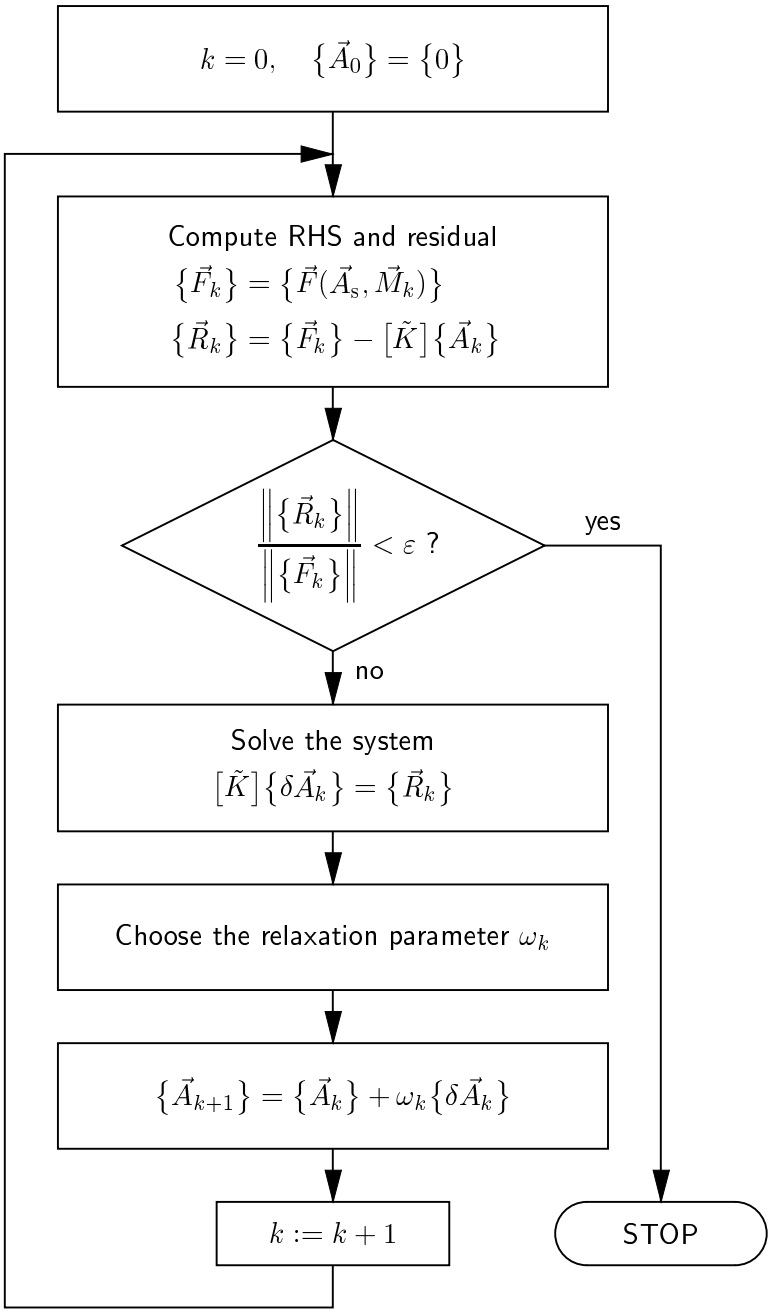

Fig. 3: $M(B)$-iteration

then to be replaced by

$$\{\vec{A}_{k+1}\} = \{\vec{A}_k\} + \omega_k \{\delta\vec{A}_k\}. \tag{55}$$

With the techniques given in [7] it can be shown that the $M(B)$-iteration converges for $0 < \omega_k < 2$. However, practical experiments showed that a considerable speed-up can be achieved by an adaptive computation of the relaxation parameter from the increment of the current and the previous iteration step according to [6, 8]

$$\left.\begin{aligned} &\omega_0 = 1, \\ &\omega_k = \frac{\omega_{k-1}}{1 - \dfrac{\{\delta\vec{A}_k\} \cdot \{\delta\vec{A}_{k-1}\}}{\left\|\{\delta\vec{A}_{k-1}\}\right\|^2}}, \quad k = 1, 2, \dots \end{aligned}\right\}. \tag{56}$$

Figure 3 shows the flowchart of the $M(B)$-iteration. A suitable stopping criterion is $\varepsilon = 10^{-4} \dots 10^{-5}$. Compared to the widespread Newton-Raphson method, the $M(B)$-iteration has the following advantages:

- The system matrix $\left[\tilde{K}\right]$ has to be assembled and factorized only once, provided that a direct solver is used.
- The special structure of $\left[\tilde{K}\right]$ shown in (50) is preserved. Thus the numerical expense is that of a scalar potential problem, because only the subblock $\left[K\right]$ has to be processed.
- The $M(B)$-method is globally convergent.
- No derivatives of the magnetization curve (4) are required.

Of course, there are also disadvantages:

- The required number of iteration steps is much higher. The 3D problem presented in [6] took about 200 steps.
- Even in the case of linear media the $M(B)$-iteration is necessary.

7 Superconducting Magnet Field Calculation

In this section, the BEM-FEM coupling is applied to the field calculation of superconducting dipole magnets. These are the main dipole magnets of the Large Hadron Collider. The Large Hadron Collider is a superconducting accelerator for protons and heavy ions to be installed at CERN. The Large Hadron Collider will be placed in an existing tunnel with a circumference of about 27 km. Space limitations as well as cost considerations dictate a two-in-one magnet design, where the two rings are incorporated in the same cryostat. The main dipole magnets will operate at about 0.58 T at injection and 8.40 T at nominal current. The superconducting magnets are characterized by the dominance of the coil geometry for the field distribution. The design goals for the magnets are maximum dipole field, minimum content of unwanted multipoles and sufficient safety margin for the conductor over the whole operation range.
Figure 4 shows a cross-section of the magnet. For symmetry reasons, only a quarter of the geometry needs to be considered as shown in Figure.
The aim of the numerical analysis is to determine the quality of the magnetic field. For this purpose, the radial component B_r of the magnetic induction is expanded into a multipole series with respect to the center $(x_0, y_0) = (\mathsf{beam2}, 0)$ of the coil,

$$B_r(r, \varphi) = \sum_{n=1}^{\infty} r^{n-1}\big(B_n \sin(n\varphi) + A_n \cos(n\varphi)\big). \tag{57}$$

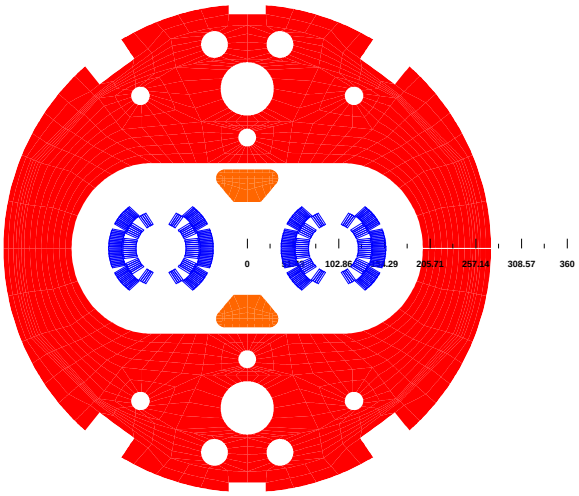

Fig. 4: Cross-section of the magnet showing the superconducting coils, the iron yoke and the iron inserts.

The B_n are called the normal and the A_n the skew components of the field. By introducing the normal and skew relative field components

$$b_n = \frac{B_n}{B_1} r_0^{n-1}, \quad a_n = \frac{A_n}{B_1} r_0^{n-1}, \tag{58}$$

(57) can be written in the form

$$B_r(r,\varphi) = B_1 \sum_{n=1}^{\infty} \left(\frac{r}{r_0}\right)^{n-1} \big(b_n \sin(n\varphi) + a_n \cos(n\varphi)\big). \tag{59}$$

B_1 is the main field component ($b_1 = 1$) and r_0 a given radius. At $r = r_0$ we have

$$B_r(r_0,\varphi) = B_1 \sum_{n=1}^{\infty} \big(b_n \sin(n\varphi) + a_n \cos(n\varphi)\big). \tag{60}$$

The numerical computation of the relative multipole components is a challenging task [9]. These components are of the order 10^{-4}. Even to obtain three valid digits, the accuracy of the field computation has to be of the order 10^{-6}. One basic requirement is the correct modelling of the coils, which have a complicated geometry and current density distribution. As can be seen from (50), the input data for the BEM-FEM coupling is the vector potential $\{\vec{A}_s\}$ of the source currents at the locations of the boundary nodes. This can easily be obtained from the design data of the coils. The design and optimization of the coil geometry has been performed with the CERN program package ROXIE [10]. From the ROXIE database, the location and current of each filamentary conductor is available. For the ν-th conductor located at $\vec{x}_\nu$ and carrying the current I_ν we get from (39)

$$\vec{A}_{s,\nu}(\vec{\xi}) = \mu_0 I_\nu u^*(\vec{x}_\nu, \vec{\xi}). \tag{61}$$

For the numerical analysis, the magnet is assumed to be infinitely extended in z-direction. The resulting 2D problem is described by (46). Only a quarter of the geometry needs to be discretized when the symmetry is taken into account by the boundary condition

$$\frac{\partial A_z}{\partial n} = 0 \tag{62}$$

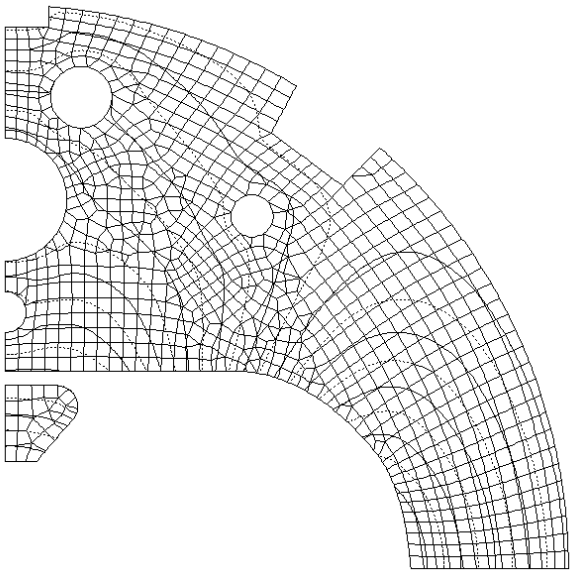

Fig. 5: Coarse mesh with 3396 nodes and computed $\vec{B}$-field

on both coordinate axis. This means that the modified fundamental solution

$$\begin{aligned}\tilde{u}^*(x,y,\xi,\eta) &= u^*(x,y,\xi,\eta) + u^*(x,y,-\xi,\eta) \\ &\quad + u^*(x,y,\xi,-\eta) + u^*(x,y,-\xi,-\eta)\end{aligned} \tag{63}$$

has to be used for the computation of the matrices $\big[G\big]$ and $\big[H\big]$. Only the iron yoke and the iron insert need to be meshed. We used 8-noded quadrilateral and 6-noded triangular second order finite elements and 3-noded second order boundary line elements. A coarse mesh with 3396 nodes (Figure 5) and a fine mesh with 6521 nodes have been considered.

Once the field problem has been solved, the relative multipole components according to (60) can be evaluated. For this purpose, the magnetic vector potential $A_z(r_0,\varphi)$ is required on a circle C with the center $(x_0,y_0) = (\mathsf{beam2},0)$ and the radius $r_0 = 10$ mm. This can be done by evaluating (40) in terms of the boundary element discretization. The potential

$$A_z(\vec{\xi}) = A_{z\mathrm{s}}(\vec{\xi}) + \underbrace{\Big(-\oint\limits_{\Gamma_{\mathrm{BEMi}}} Q_z\, u^*\,\mathrm{d}\Gamma - \oint\limits_{\Gamma_{\mathrm{BEMi}}} A_z\, q^*\,\mathrm{d}\Gamma\Big)}_{=\,A_{z\mathrm{r}}(\vec{\xi})}, \quad \vec{\xi}\in C \tag{64}$$

consists of two parts: The impressed potential $A_{z\mathrm{s}}$ due to the coils and the **reduced potential** $A_{z\mathrm{r}}$ due to the magnetization [9]. The potential $A_z(\vec{\xi})$ has been evaluated in 144 discrete points on C at an angular distance of $\Delta\varphi = 2.5°$. With these sample values a discrete harmonic analysis has been performed by means of the program TRICOF from the CERN Library. TRICOF yields the coefficients p_n and q_n of the Fourier expansion

$$A_z(r_0,\varphi) = \frac{p_0}{2} + \sum_{n=1}^{\infty}\big(p_n\cos(n\varphi) + q_n\sin(n\varphi)\big). \tag{65}$$

Taking into account

$$B_r(r_0,\varphi) = \frac{1}{r_0}\frac{\partial}{\partial\varphi}A_z(r_0,\varphi) \tag{66}$$

	Coarse Mesh $B_1 = -7.64289$ T	Fine Mesh $B_1 = -7.64290$ T
n	b_n	b_n
2	1.45900·10^{-4}	1.46035·10^{-4}
3	-1.11400·10^{-4}	-1.11413·10^{-4}
4	-0.15273·10^{-4}	-0.15269·10^{-4}
5	-0.19984·10^{-4}	-0.19983·10^{-4}
6	0.00432·10^{-4}	0.00432·10^{-4}
7	0.03386·10^{-4}	0.03385·10^{-4}
8	-0.00153·10^{-4}	-0.00153·10^{-4}
9	-0.01062·10^{-4}	-0.01062·10^{-4}
10	0.00165·10^{-4}	0.00166·10^{-4}
11	0.00919·10^{-4}	0.00918·10^{-4}

Table 1: Relative multipole components for the coarse and the fine mesh (Stopping criterion $\varepsilon = 10^{-6}$)

the a_n, b_n can be expressed in terms of the p_n, q_n according to

$$B_1 = -\frac{p_1}{r_0}, \quad b_n = -\frac{np_n}{r_0 B_1}, \quad a_n = \frac{nq_n}{r_0 B_1}. \tag{67}$$

Starting from the expansion (65) and using the relations (67) avoids numerical differentiation of the vector potential.

Due to the symmetry we have $a_n = q_n = 0$. Table 1 contains the results for the coarse and the fine mesh. Even with the coarse mesh the first four digits can be regarded as accurate.

The high accuracy requirements in connection with the high saturation level of the iron pose a demanding test on the $M(B)$-iteration. Table 2 shows the results for the coarse mesh and different stopping criteria ε. The higher order multipoles b_7, b_9, b_{11} are hardly influenced by the yoke and the iron saturation effect. The estimates for a coil in an infinite permeable iron yoke are $b_7 = 0.034 \cdot 10^{-4}$, $b_9 = -0.010 \cdot 10^{-4}$, and $b_{11} = 0.0088 \cdot 10^{-4}$ [9]. These multipoles are therefore a good measure of the accuracy of the field solution. Indeed, Table 2 shows a good agreement with the predicted values and no dependency on the stopping criterion. The quadrupole b_2, which results from the two-in-one design depends on the stopping criterion. The first four digits can be regarded as exact for $\varepsilon \leq 10^{-5}$. It should be noted that an unnecessarily strict stopping criterion results in an excessive high number of iterations (up to 1400 iterations for $\varepsilon = 10^{-6}$, up to 2000 iterations for $\varepsilon = 10^{-7}$).

8 Conclusion

This paper presented a detailed explanation of the BEM-FEM coupling for nonlinear magnetostatic problems. The proposed method was applied to the computation of the multipole errors in the field of a superconducting dipole magnet. The exciting coils need not to be discretized, but their vector potential can directly be used as input data for the field computation. The reduced vector potential due to the magnetization was computed by integration over the BEM-FEM coupling interface, which tends to smooth out local errors.

REFERENCES

[1] S. Kurz, J. Fetzer, G. Lehner, and W.M. Rucker. Die Anwendung der BEM - FEM - Kopplungsmethode zur Behandlung dreidimensionaler nichtlinearer Abschirmungsprobleme niederfrequenter Felder am Beispiel des TEAM Problems 21. *Archiv für Elektrotechnik*, 80(2):91–104, 1997.

	$\varepsilon = 10^{-4}$	$\varepsilon = 10^{-5}$	$\varepsilon = 10^{-6}$	$\varepsilon = 10^{-7}$
	$B_1 = -7.64282$ T	$B_1 = -7.64288$ T	$B_1 = -7.64289$ T	$B_1 = -7.64289$ T
n	b_n	b_n	b_n	b_n
2	$1.45156 \cdot 10^{-4}$	$1.45851 \cdot 10^{-4}$	$1.45900 \cdot 10^{-4}$	$1.45902 \cdot 10^{-4}$
3	$-1.11370 \cdot 10^{-4}$	$-1.11397 \cdot 10^{-4}$	$-1.11400 \cdot 10^{-4}$	$-1.11400 \cdot 10^{-4}$
4	$-0.15274 \cdot 10^{-4}$	$-0.15273 \cdot 10^{-4}$	$-0.15273 \cdot 10^{-4}$	$-0.15273 \cdot 10^{-4}$
5	$-0.19984 \cdot 10^{-4}$	$-0.19984 \cdot 10^{-4}$	$-0.19984 \cdot 10^{-4}$	$-0.19984 \cdot 10^{-4}$
6	$0.00432 \cdot 10^{-4}$	$0.00432 \cdot 10^{-4}$	$0.00432 \cdot 10^{-4}$	$0.00432 \cdot 10^{-4}$
7	$0.03386 \cdot 10^{-4}$	$0.03386 \cdot 10^{-4}$	$0.03386 \cdot 10^{-4}$	$0.03386 \cdot 10^{-4}$
8	$-0.00153 \cdot 10^{-4}$	$-0.00153 \cdot 10^{-4}$	$-0.00153 \cdot 10^{-4}$	$-0.00153 \cdot 10^{-4}$
9	$-0.01062 \cdot 10^{-4}$	$-0.01062 \cdot 10^{-4}$	$-0.01062 \cdot 10^{-4}$	$-0.01062 \cdot 10^{-4}$
10	$0.00166 \cdot 10^{-4}$	$0.00165 \cdot 10^{-4}$	$0.00165 \cdot 10^{-4}$	$0.00166 \cdot 10^{-4}$
11	$0.00919 \cdot 10^{-4}$	$0.00919 \cdot 10^{-4}$	$0.00919 \cdot 10^{-4}$	$0.00919 \cdot 10^{-4}$

Table 2: Relative multipole components for different stopping criteria ε (coarse mesh)

[2] M. Javid and P.M. Brown. *Field Analysis and Electromagnetics.* McGraw-Hill Electrical and Electronic Engineering Series. McGraw-Hill Book Company, New York, 1963.

[3] C. Brebbia, J. Telles, and L. Wrobel. *Boundary Element Techniques.* Springer-Verlag, Berlin, 1984.

[4] J. Fetzer. *Die Lösung statischer und quasistationärer elektromagnetischer Feldprobleme mit Hilfe der Kopplung der Methode der finiten Elemente und der Randelementmethode.* PhD thesis, Universität Stuttgart, VDI Verlag Düsseldorf, 1995.

[5] S. Kurz, J. Fetzer, and G. Lehner. An improved algorithm for the BEM-FEM-coupling method using domain decomposition. *IEEE Transactions on Magnetics*, 31(3):1737–1740, May 1995.

[6] S. Kurz, J. Fetzer, and G. Lehner. A novel iterative algorithm for the nonlinear BEM-FEM coupling method. *IEEE Transactions on Magnetics*, 33(2):1772–1775, March 1997.

[7] I. Mayergoyz. Iteration methods for the calculation of steady magnetic fields in nonlinear ferromagnetic media. *COMPEL - The International Journal for Computation and Mathematics in Electrical and Electronic Engineering*, 1(2):89–110, 1982.

[8] S. Kurz, J. Fetzer, and G. Lehner. Comparison between different iterative methods for calculation of magnetostatic fields in nonlinear media. In *Proc. of the 6th International IGTE Symposium*, pages 77–82, Graz, Austria, September 1994.

[9] C. Paul, K. Preis, and S. Russenschuck. 2d finite-element calculation of superconducting magnets applying a reduced vector potential $\vec{A}_r$-formulation. In *Proc. of the 7th International IGTE Symposium*, pages 30–36, Graz, Austria, September 1996.

[10] S. Russenschuck. Synthesis, inverse problems and optimization in computational electromagnetics. *International Journal of Numerical Modelling: Electronic Networks, Devices and Fields*, 9:45–57, 1996.